Biophysical Journal
Biophysical Letter

Biophysical Society

Are Filopodia Privileged Signaling Structures in Migrating Cells?

Heath E. Johnson[1] and Jason M. Haugh[1,*]
[1]Department of Chemical and Biomolecular Engineering, North Carolina State University, Raleigh, North Carolina

ABSTRACT Filopodia are thin, fingerlike structures that contain bundled actin filaments and project from the cell periphery. These structures are dogmatically endowed with the ability to sense cues in the microenvironment, implying that filopodia foster local signal transduction, yet their small diameter hampers the imaging of dynamic processes therein. To overcome this challenge, we analyzed total internal reflection fluorescence images of migrating fibroblasts coexpressing either a plasma membrane marker or tagged AktPH domain, a translocation biosensor for signaling through the phosphoinositide 3-kinase pathway, along with a cytosolic volume marker. We devised a scheme to estimate the radii of filopodia using either the membrane marker or volume marker data, and we used that information to account for geometry effects in the biosensor data. With conservative estimates of relative target molecule abundance, it is revealed that filopodia typically harbor higher densities of 3′ phosphoinositides than adjacent regions at the cell periphery. In this context at least, the analysis supports the filopodial signaling hypothesis.

In migrating cells, various cytoskeletal arrays assemble in concert with motor proteins to generate forces that drive cell locomotion. At the leading edge of a motile cell, two prominent F-actin architectures are typically observed: the dendritic actin network that is characteristic of broad protrusions (lamellipodia), and bundled actin filaments that are typically present in thin (~100 nm diameter), fingerlike projections called filopodia (1). Both structures promote formation of adhesion complexes, which in turn interact with F-actin as a mechanical clutch (2,3). Adhesion complexes also mediate signal transduction, which affects F-actin polymerization and myosin contractility (4).

Recently, we studied the interplay among these dynamical systems, as it relates to the coupling of adhered filopodia and the emergence of nascent lamellipodia; we showed that adhesion-based signaling mediated the coupling (5). Enriched type I phosphoinositide 3-kinase (PI3K) signaling was detected by total internal reflection fluorescence (TIRF) microscopy in filopodia before the onset of lamellipodial protrusion, using fluorescent protein-tagged Akt PH domain (AktPH) as a translocation biosensor; however, we were unable to interpret the intensity data in terms of the density of AktPH recruited to filopodia. The analysis was confounded because the entirety of a thin filopod might be significantly excited by TIRF, exaggerating the membrane-bound contribution to the intensity (Fig. 1). Accounting for this effect of filopod geometry is the rationale for this study.

TIRF illumination selectively excites fluorophores in close proximity to a glass-aqueous interface. The local fluorescence intensity, $f(x,y)$, is generally related to the fluorophore concentration, $[F](x,y,z)$, as follows (6):

$$f(x,y) = \alpha \int_0^\infty [F] e^{-z/d} dz. \quad (1)$$

The penetration depth, d ~100 nm, describes the decay of TIRF excitation with distance from the surface, z; d is proportional to the excitation wavelength and readily calculated (6). The coefficient α accounts for the properties of the fluorophore and of the image acquisition.

If we consider a translocation biosensor such as AktPH, a fraction of it is in complex with its target(s) at the plasma membrane, and a fraction resides in the adjacent cytoplasm. Using the notation of Haugh (7), we take the local concentration of unbound biosensor as $[B]$ and the local density of membrane-bound complex as C. For a semiinfinite region, such as the center of the cell, and a gap height h between the glass surface and the cell, Eq. 1 is solved as follows (6):

$$f = \alpha e^{-h/d}(d[B] + C). \quad (2)$$

The solution of Eq. 1 for a different geometry is not as straightforward. To compare the TIRF intensities of

Submitted June 6, 2016, and accepted for publication September 19, 2016.
*Correspondence: jason_haugh@ncsu.edu
Editor: Philip LeDuc.
http://dx.doi.org/10.1016/j.bpj.2016.09.022

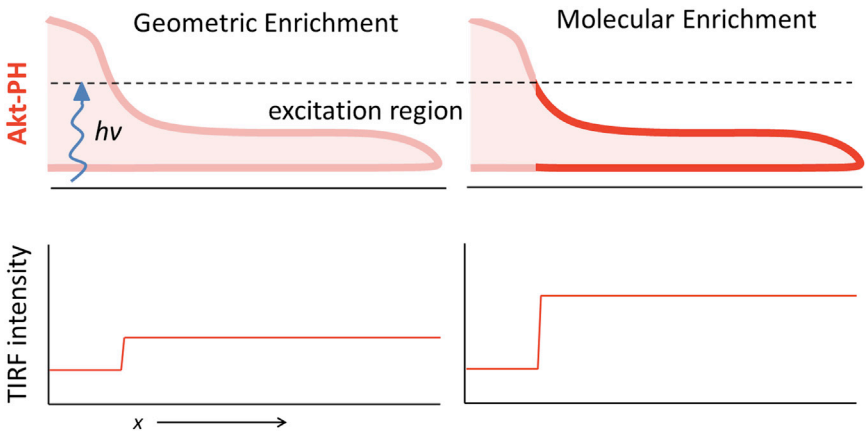

FIGURE 1 Illustration of enrichment due to filopod geometry versus enrichment of bound biosensor. To see this figure in color, go online.

individual filopodia to that of a semiinfinite region, their geometries must be taken into account (Fig. 2 *A*). In the analyses presented here, we consider each filopod as a cylinder with length, L, and radius, R, with the latter typically below the limit of optical resolution.

A cohort of nine mouse fibroblasts (NIH3T3; American Type Culture Collection, Manassas, VA) that coexpressed GPI-tdTomato, a membrane marker, and cytosolic teal fluorescent protein (TFP) were imaged by TIRF microscopy as reported in Johnson et al. (5). For each filopod ($n = 1{,}916$) and marker, we determined the dimensionless quantity, Φ, defined here as follows:

$$\Phi = \frac{f_f}{f_c}\frac{A_f}{dL}. \tag{3}$$

Here, f_f and A_f are the mean intensity and area of the filopod region, and f_c is the mean intensity of the cell center (see Supporting Materials and Methods and Fig. S1 in the Supporting Material). Each filopod was tracked over sequential frames (5), and the measured value of Φ is an average over the filopod's lifetime. Assuming a uniform membrane marker and our geometric model, and neglecting the possible difference in h between the two regions, we derived an expression for Φ as a function of $\rho = R/d$. We refer to this function as Φ_{mem} (all derivations are provided in Supporting Materials and Methods):

$$\Phi_{\mathrm{mem}} = 2\pi\rho e^{-\rho} I_0(\rho). \tag{4}$$

We applied this model to the GPI-tdTomato data (with d for 561 nm excitation) to estimate R for each filopod (Fig. 2 *B*). The distribution peaks at $\approx$50 nm, consistent with ultrastructural measurements (1). For the cytosolic marker, TFP, we similarly derived an equation for Φ, Φ_{cyt} (with d for 442 nm excitation):

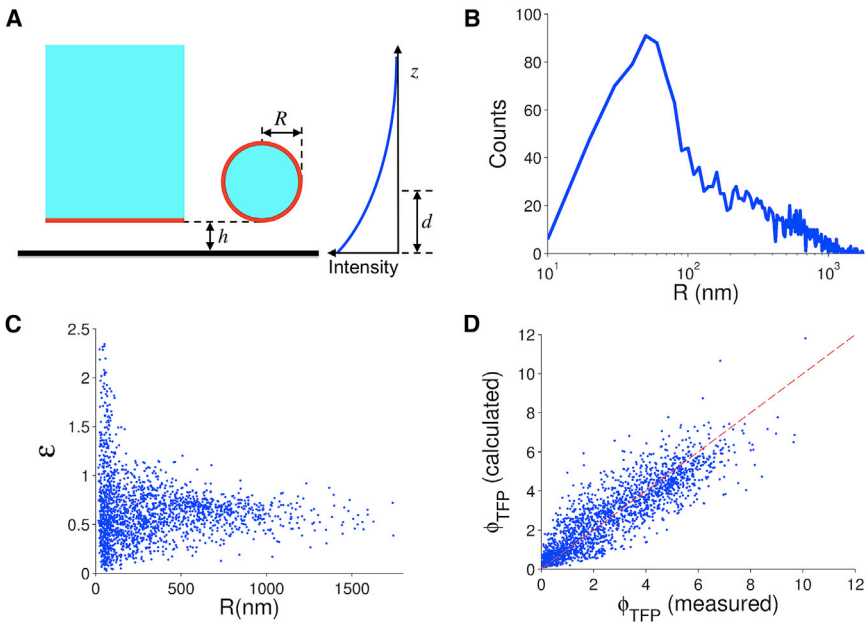

FIGURE 2 Properties of adhered filopodia inferred from TIRF images. (*A*) Illustration of TIRF illumination for a semiinfinite region of a cell versus the circular cross section of a filopod. (*B*) Histogram of filopod radii determined from images of the membrane marker, GPI-tdTomato. (*C*) With R determined from b, the volume marker (TFP) images were used to estimate the void fraction ε_f for each filopod. (*D*) With R determined from b and assuming $\varepsilon_f = 0.62$ for each filopod, the predicted value of Φ for the volume marker (Eq. 5) is compared to the measured value. To see this figure in color, go online.

$$\Phi_{cyt} = 2\pi\varepsilon_f \rho e^{-\rho} I_1(\rho). \quad (5)$$

The coefficient ε_f was added to account for the void fraction inside filopodia (relative to the cytosol in the center region). Using the values of R estimated from the GPI-tdTomato data, the values of ε_f were estimated from the TFP data. The results reveal a reasonable peak ε_f value of 0.62, with large variability only among filopodia with the lower estimates of R (Fig. 2 *C*). Supposing that the mean value of ε_f were assumed for all filopodia, and using the same estimates of R from before, the values of Φ for TFP were predicted (Eq. 5) and compared to the measured values. A reasonable agreement was found (Fig. 2 *D*; coefficient of determination = 0.72). We conclude that our geometric model is suitable for characterizing filopodia.

In another group of 21 cells coexpressing mCherry-AktPH and TFP, a total of 1336 filopodia were identified. This data set extends one described previously in Johnson et al. (5). To relate the measured TIRF intensity to the abundance of AktPH in filopodia, we combine the results given above to derive Φ for a translocation biosensor:

$$\Phi = \frac{d[B]_f \Phi_{cyt} + C_f \Phi_{mem}}{d[B]_c + C_c}. \quad (6)$$

Equation 6 is simplified by assuming: biosensor-target binding at the center of the cell, C_c, is negligible; free biosensor is fast diffusing and therefore close to uniform ($[B]_f \approx [B]_c$); and biosensor-target binding is close to equilibrium. Therefore,

$$\Phi = \Phi_{cyt} + \left(T_f / dK_D\right)\Phi_{mem}, \quad (7)$$

where T_f is the density of (unbound) target in the filopod membrane, and K_D is the equilibrium dissociation constant of biosensor-target binding. With prior estimates of ρ and ε_f, Eq. 7 allows estimation of T_f/dK_D, a dimensionless measure of target abundance. The underlying assumptions are conservative. If there were substantial target density in filopodia, then local depletion of free biosensor is expected ($[B]_f < [B]_c$) (7); accounting for this, and allowing C_c to be significant, would only increase the estimate of T_f/dK_D.

Assuming a value of $\varepsilon_f = 0.62$ based on the analysis shown in Fig. 1, *C* and *D*, the TFP data for this cohort

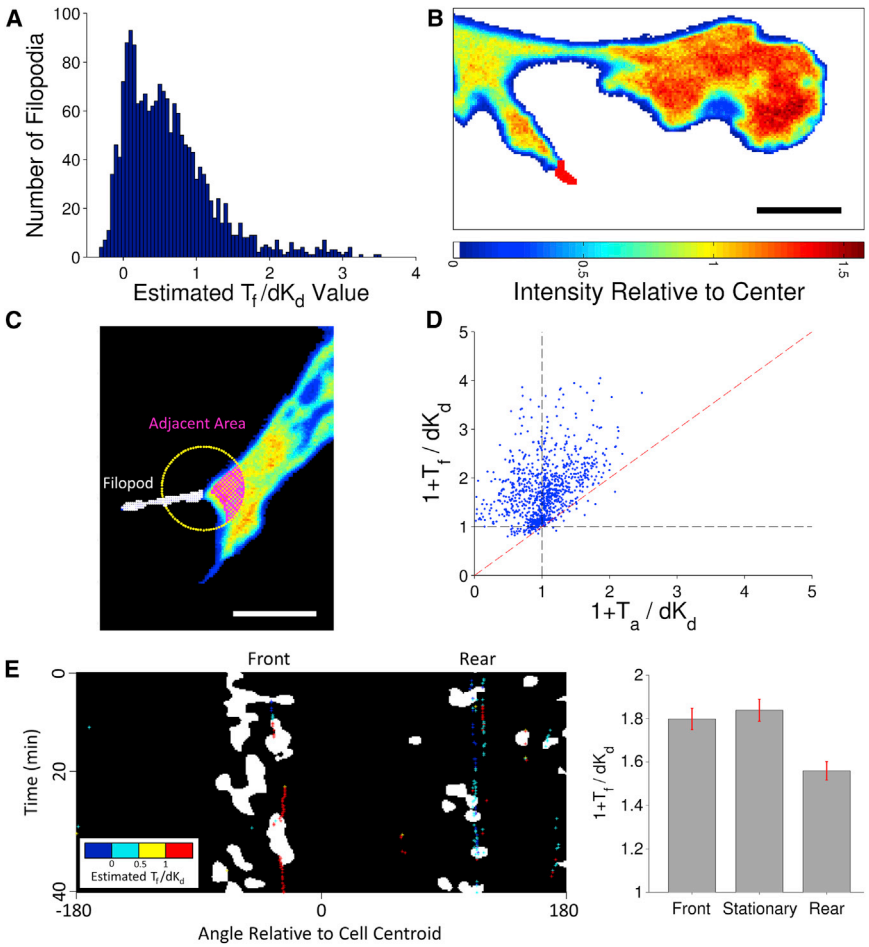

FIGURE 3 Quantifying PI3K signaling in filopodia. (*A*) Histogram of T_f/dK_D estimated from Eq. 7. (*B*) Adjusted fluorescence intensity of a filopod (*arrow*). Scale bar = 10 μm. (*C*) Pseudocolor TIRF image showing the specification of a region adjacent to a filopod. Scale bar = 10 μm. (*D*) The adjusted fluorescence of each filopod, $1+T_f/dK_D$, is compared to that of the adjacent region, $1+T_a/dK_D$. (*E*) Spatiotemporal map showing structures identified as lamellipodia (*white*) and filopodia (colored according to T_f/dK_D). (*Right*) The bar graph shows the mean adjusted intensities of filopodia associated with front (n = 310), stationary (n = 547), and rear (n = 479) regions (see also Fig. S2). The error bars are 95% confidence intervals. To see this figure in color, go online.

yielded estimates of R for all filopodia. Turning to the mCherry-AktPH data, the assumed value of ε_f and the estimated value of R were used to estimate T_f/dK_D for each filopod (Eq. 7, with d for 561 nm excitation). As expected, the vast majority of the T_f/dK_D values are substantially positive (Fig. 3 *A*). Each T_f/dK_D value can, in turn, be used to conservatively estimate an adjusted fluorescence, as if the filopod were flat and semiinfinite, comparable to intensities elsewhere in the contact area (Fig. 3 *B*):

$$f_{f,\text{adjusted}} = f_c\left(1 + T_f/dK_D\right). \quad (8)$$

With this approach, we compared the adjusted intensity of each filopod, $1+T_f/dK_D$, to that of the adjacent region, $1+T_a/dK_D$ (Fig. 3 *C*; see Supporting Materials and Methods). According to this analysis, most filopodia (94%) showed enrichment of AktPH binding, even when the adjacent regions did not, and with few exceptions the enrichment in the filopod exceeded that of the adjacent region (95%; Fig. 3 *D*).

To put this analysis in a dynamic context, a spatiotemporal map constructed from a time series of a representative cell displays the timing and locations of structures identified as lamellipodia and filopodia (Fig. 3 *E*) (5). In this sequence, a prominent filopod at the front of the cell adhered before the emergence of a lamellipod, consistent with our previous findings (5); this filopod showed strong enrichment of AktPH binding. At the same time, structures identified as filopodia (but exhibiting hallmarks of retraction fibers) were present at the trailing end of the cell and exhibited low enrichment of AktPH binding. The latter observation prevailed overall for filopodia emanating from regions identified as retracting (Figs. 3 *E* and S2).

Filopodia are broadly described as environmental sensors (1,8), implying that signals are transduced from within. Here we have outlined a method for estimating the enrichment of fluorescent biosensors in adhered filopodia. We offer evidence that adhered filopodia of fibroblasts are indeed privileged loci for PI3K signaling, as inferred for neurons (9). Whether filopodia foster activation of PI3K or frustrate dephosphorylation of its lipid products remains to be explored. An alternate explanation is that filopodia offer a longer domain for lipid accumulation; the added length would ameliorate dilution by diffusion of the lipid away from the leading edge. This is plausible because we previously estimated a spatial range of ~10 μm for this second messenger (10), substantially larger than the thickness of the dendritic F-actin network at the cell's leading edge(s).

SUPPORTING MATERIAL

Supporting Materials and Methods and two figures are available at http://www.biophysj.org/biophysj/supplemental/S0006-3495(16)30822-0.

AUTHOR CONTRIBUTIONS

H.E.J. performed research, and both authors designed research, analyzed data, and wrote the article.

ACKNOWLEDGMENTS

This work was supported by grant No. R01-GM110155 from the National Institutes of Health.

REFERENCES

1. Mattila, P. K., and P. Lappalainen. 2008. Filopodia: molecular architecture and cellular functions. *Nat. Rev. Mol. Cell Biol.* 9:446–454.
2. Galbraith, C. G., K. M. Yamada, and J. A. Galbraith. 2007. Polymerizing actin fibers position integrins primed to probe for adhesion sites. *Science.* 315:992–995.
3. Chan, C. E., and D. J. Odde. 2008. Traction dynamics of filopodia on compliant substrates. *Science.* 322:1687–1691.
4. Vicente-Manzanares, M., C. K. Choi, and A. R. Horwitz. 2009. Integrins in cell migration—the actin connection. *J. Cell Sci.* 122:199–206.
5. Johnson, H. E., S. J. King, …, J. M. Haugh. 2015. F-actin bundles direct the initiation and orientation of lamellipodia through adhesion-based signaling. *J. Cell Biol.* 208:443–455.
6. Reichert, W. M., and G. A. Truskey. 1990. Total internal reflection fluorescence (TIRF) microscopy. I. Modelling cell contact region fluorescence. *J. Cell Sci.* 96:219–230.
7. Haugh, J. M. 2012. Live-cell fluorescence microscopy with molecular biosensors: what are we really measuring? *Biophys. J.* 102:2003–2011.
8. Davenport, R. W., P. Dou, …, S. B. Kater. 1993. A sensory role for neuronal growth cone filopodia. *Nature.* 361:721–724.
9. Luikart, B. W., W. Zhang, …, L. F. Parada. 2008. Neurotrophin-dependent dendritic filopodial motility: a convergence on PI3K signaling. *J. Neurosci.* 28:7006–7012.
10. Schneider, I. C., E. M. Parrish, and J. M. Haugh. 2005. Spatial analysis of 3′ phosphoinositide signaling in living fibroblasts, III: influence of cell morphology and morphological polarity. *Biophys. J.* 89:1420–1430.

Biophysical Journal, Volume *111*

Supplemental Information

Are Filopodia Privileged Signaling Structures in Migrating Cells?

Heath E. Johnson and Jason M. Haugh

Supplementary Material
Are filopodia privileged signaling structures in migrating cells?

by Heath E. Johnson and Jason M. Haugh

Text S1: Methods supplement

Derivation of filopodial fluorescence, membrane marker (Eq. 4)

We first consider a uniformly distributed membrane marker with area density M. Referring to the geometry illustrated in Fig. 1A, we adopt polar coordinates (r,θ), with $\theta = 0$ pointed in the $+z$-direction, and hence we express z as follows.

$$z = h + R + r\cos\theta$$

The total background-subtracted fluorescence 'volume' of the filopod, given by $f_f A_f$, is calculated by integrating over the volume of the cylinder, weighting by $e^{-z/d}$ as shown in Eq. 1 of the main text. Since the fluorophore is confined to the boundary at $r = R$, we invoke the Dirac delta function, $\delta(x)$, and express the integral as follows.

$$f_f A_f = \alpha M\left[2\int_0^R\int_0^\pi \delta(r-R)e^{-(h+R+r\cos\theta)/d}\,r\,dr\,d\theta\right]L$$

$$= 2\alpha e^{-(h+R)/d}MRL\int_0^\pi e^{-R\cos\theta/d}\,d\theta$$

The fluorescence intensity at the center of the cell is simply

$$f_c = \alpha M\int_0^\infty \delta(z-h)e^{-z/d}\,dz$$

$$= \alpha e^{-h/d}M$$

And so the expression for Φ as defined in the main text is found.

$$\Phi = \frac{f_f A_f}{f_c dL} = 2\rho e^{-\rho}\int_0^\pi e^{-\rho\cos\theta}\,d\theta; \quad \rho = \frac{R}{d}$$

Finally, an integral identity for $I_0(x)$, a modified Bessel function of the first kind, is applied.

$$I_0(x) = \frac{1}{\pi}\int_0^\pi e^{x\cos\theta}\,d\theta = \frac{1}{\pi}\int_0^\pi e^{-x\cos\theta}\,d\theta$$

This yields the expression for Φ_{mem} given as Eq. 4 in the main text.

Derivation of filopodial fluorescence, volume marker (Eq. 5)

Following the same approach as above, now for a uniformly distributed volume marker with concentration $[F]$, we obtain the following. Note that the constant void fraction ε_f has been assumed for the filopod.

$$f_f A_f = \alpha\varepsilon_f[F]\left[2\int_0^R\int_0^\pi e^{-(h+R+r\cos\theta)/d}\,r\,dr\,d\theta\right]L$$

$$= 2\alpha e^{-(h+R)/d}\varepsilon_f[F]L\int_0^R\int_0^\pi e^{-r\cos\theta/d}\,r\,dr\,d\theta;$$

$$f_c = \alpha e^{-h/d}[F]d;$$

$$\Phi = \frac{2\varepsilon_f e^{-\rho}}{d^2}\int_0^R\int_0^\pi e^{-r\cos\theta/d}\,r\,dr\,d\theta$$

Invoking the properties of Bessel functions, the above is evaluated as follows.

$$\Phi = \frac{2\pi\varepsilon_f e^{-\rho}}{d^2}\int_0^R I_0(r/d)\,r\,dr$$
$$= 2\pi\varepsilon_f e^{-\rho}\rho I_1(\rho)$$

This is equivalent to the expression for Φ_{cyt} given as Eq. 5 in the main text.

Derivation of filopodial fluorescence, translocation biosensor (Eq. 6)

For a translocation biosensor, with average free concentration $[B]_f$ and average membrane-bound density C_f in the filopod, we apply the same approach and results from above to calculate total fluorescence.

$$f_f A_f = 2\alpha e^{-(h+R)/d} L\left(\varepsilon_f [B]_f \int_0^R \int_0^\pi e^{-r\cos\theta/d} r\,dr\,d\theta + C_f R\int_0^\pi e^{-R\cos\theta/d}\,d\theta\right)$$
$$= 2\pi\alpha e^{-(h+R)/d} L\left(\varepsilon_f [B]_f d^2\rho I_1(\rho) + C_f R I_0(\rho)\right)$$
$$= \alpha e^{-h/d} Ld\left(d[B]_f \Phi_{cyt} + C_f \Phi_{mem}\right)$$

Invoking Eq. 2 for the fluorescence intensity at the cell center, f_c, and combining with the above yields the expression for Φ given as Eq. 6 in the main text.

Specification of *d* values for various excitation wavelengths

The characteristic penetration depth (d) of an evanescent wave can be estimated from the excitation wavelength (λ = 442 nm for TFP, 561 nm for tdTomato and mCherry), the angle of incidence of the beam ($\theta_i \approx 70°$), and the refractive indices of glass (n_1 = 1.52) and aqueous solutions (n_2 = 1.33) as follows.

$$d = \frac{\lambda}{4\pi\left(n_1^2 \sin^2\theta_i - n_2^2\right)^{1/2}}$$

Thus, d values of 68 nm and 86 nm were calculated for TFP and tdTomato/mCherry, respectively.

Image acquisition and processing

Live-cell imaging by TIRF microscopy and image processing were performed as described previously (1), and additional details are provided here. The XY optical resolution is set by the pixel side length of 256 nm (based on the pixel density of the camera and the overall magnification). Supplementary Figure S1 illustrates the image analysis workflow for a representative cell, starting with a raw image among many in a stack of sequential images (Fig. S1A). The filopodia and (non-filopodial) cell region were identified as described previously, and the center region of the cell was determined. In brief, filopodia were identified using a tophat filter applied to the binary cell mask, healing discontinuities and removing structures smaller than 15 pixels. The center region was then determined by subtracting filopodia masks from the cell mask and eroding it further by a 2.5 μm diameter disk (Fig. S1B). The filopodia were tracked across sequential images as described previously (1).

For the analysis presented in this paper, the region associated with each filopod in each image was determined by dilating the filopod mask in the TFP channel (Fig. S1C). This

step is important because it ensures that all of the filopod's fluorescence is captured, and because there is a slight focal difference between wavelengths. The area A_f associated with each filopod region (in nm^2, based on the square of the pixel side length) and the mean background-subtracted intensity of that region, f_f, were determined. Note that the background fluorescence is already subtracted, so the value of the total fluorescence, $f_f A_f$, is not sensitive to the degree of dilation. Finally, the length of each filopod, L, was estimated as the major axis of an ellipse drawn around the filopod region (without dilation). This quantity was expressed in units of nm according to the pixel side length as described above. These quantities, together with the appropriate value of d and the mean background-subtracted intensity of the center region, f_c, were used to calculate Φ for each fluorescent protein and filopod (Eq. 3). This quantity was averaged over the duration of the filopod across multiple frames (if applicable). To reduce noise, frames in which filopodia with a mean GPI or Akt-PH intensity less than 20% of the center region intensity were excluded. All calculations were executed using MATLAB (MathWorks).

Estimation of filopod radius from Φ_{mem} or Φ_{cyt} value

For cells expressing the membrane marker GPI-tdTomato, the value of Φ_{mem} for each filopod was determined from the data, and the corresponding values of ρ (Eq. 4, main text) was identified by iterative root finding. By multiplying the estimated ρ by d = 86 nm for 561-nm excitation, the estimated radius R was found. This value of R was converted back to dimensionless ρ for the TFP channel by dividing by d = 86 nm for 442-nm excitation, and then comparison of the measured Φ_{cyt} for TFP and Eq. 5 of the main text yielded an estimate of the void fraction, ε_f, for each filopod. For the cells co-expressing mCherrry-AktPH and TFP, the Φ_{cyt} for TFP was determined from the data as before, and Eq. 5 of the main text was used to estimate ρ (by iterative root finding), assuming a nominal value of ε_f = 0.62. By multiplying the estimated ρ by d = 68 nm for 442-nm excitation, the estimated radius R was found. All calculations were executed using MATLAB (MathWorks).

Specification of the contact area region adjacent to a filopod

In each applicable frame, a circle with radius 5.12 μm (corresponding to 20 pixel side-lengths), centered at the base of the filopod, was drawn. Within this circle, the non-filopodial region of the cell was identified (Fig. S1D). Prior to this, pixels that are part of the low intensity cell edge were excluded by eroding the cell mask by a 5-pixel radius disk. All operations were executed using MATLAB (MathWorks).

Calculation of adjusted intensity of the adjacent region

We used the TFP data to estimate a void fraction for the adjacent region, ε_a, relative to the center. This was taken as the ratio of the TFP intensity in the adjacent region divided by that of the center region. Then, turning to the mCherry-AktPH data, the ratio of the intensity of the adjacent region, f_a, to that of the center region (incorporating Eq. 2 from the main text) is as follows.

$$\frac{f_a}{f_c} = \frac{d\varepsilon_a[B]_a + C_a}{d[B]_c + C_c}$$

Incorporating the same assumptions as in the derivation of Eqs. 7 & 8 in the main text, we obtain

$$\frac{f_a}{f_c} = \varepsilon_a + \frac{T_a}{dK_D}$$

With f_a/f_c taken from the AktPH data and ε_a estimated from the TFP data, the ratio T_a/dK_D was estimated for each adjacent region. Hence, the adjusted fluorescence of the adjacent region was calculated as follows.

$$f_{a,adjusted} = f_c\left(1 + \frac{T_a}{dK_D}\right)$$

It suffices to compare the quantities $1+T_f/dK_D$ and $1+T_a/dK_D$ as shown in Fig. 3D of the paper. All calculations were executed using MATLAB (MathWorks).

Classification of filopodia as associated with protruding, retracting, or stationary regions

To classify cell regions based on their motility status, we calculated the relative protrusion and retraction on an angular basis about the cell centroid using overlap of cell masks between frames as described previously (2). This data was then used to generate a kymograph-like map of membrane protrusion/retraction as a function of time and angular position relative to the centroid. An averaging filter was applied to this "map" in space and time to capture only the bulk protrusion and retraction events. This smoothed protrusion/retraction map was then segmented into 3 bins using k-means clustering (Fig. S2A). The highest bin was marked as protruding, the middle one as stationary, and the bottom one as retracting. The filopodia locations were also binned with respect to angle relative to the cell centroid, and the assocated motility status of the bin for each filopod in each image was determined. Finally, each filopod was classified by whichever motility status was most frequent during the filopod lifetime.

References

1. Johnson, H. E., S. J. King, S. B. Asokan, J. D. Rotty, J. E. Bear, and J. M. Haugh. 2015. F-actin bundles direct the initiation and orientation of lamellipodia through adhesion-based signaling. J Cell Biol 208:443-455.
2. Welf, E. S., S. Ahmed, H. E. Johnson, A. T. Melvin, and J. M. Haugh. 2012. Migrating fibroblasts reorient directionality by a metastable, PI3K-dependent mechanism. J. Cell Biol. 197:105-114.

Supplementary Figures

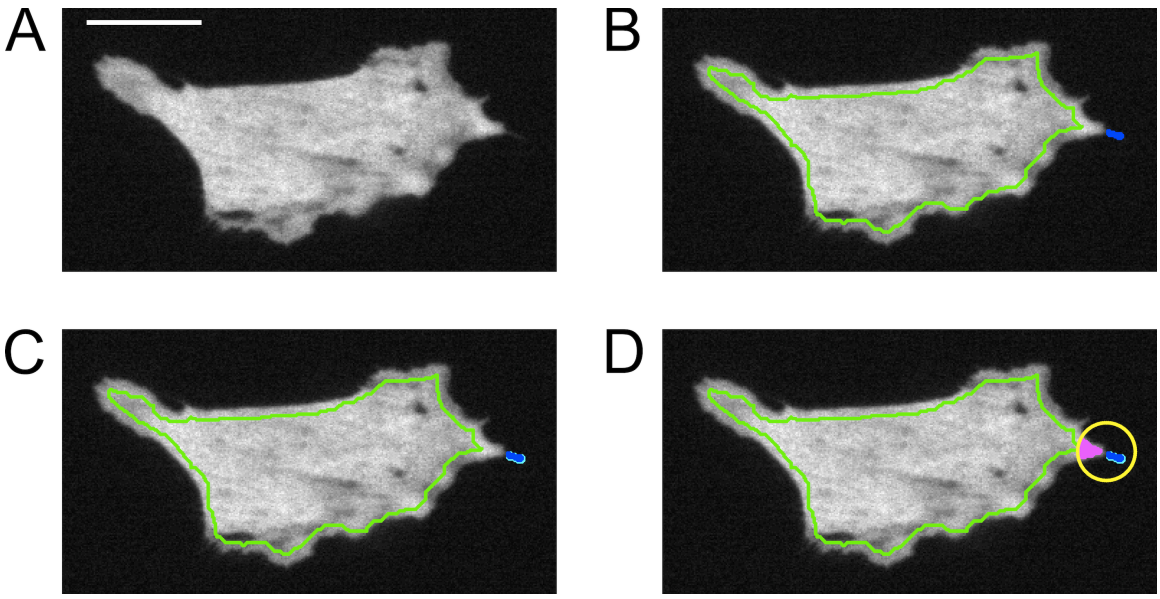

Figure S1. Identification of regions in TIRF images. *a*) TIRF image showing an entire cell expressing the volume marker, TFP. Scale bar = 20 μm. *b*) Demarcation of a filopod region (filled in blue) and the cell's center region (outlined in green). *c*) Dilation of the filopod region (extra area colored cyan). *d*) Identification of the adjacent area (filled in magenta).

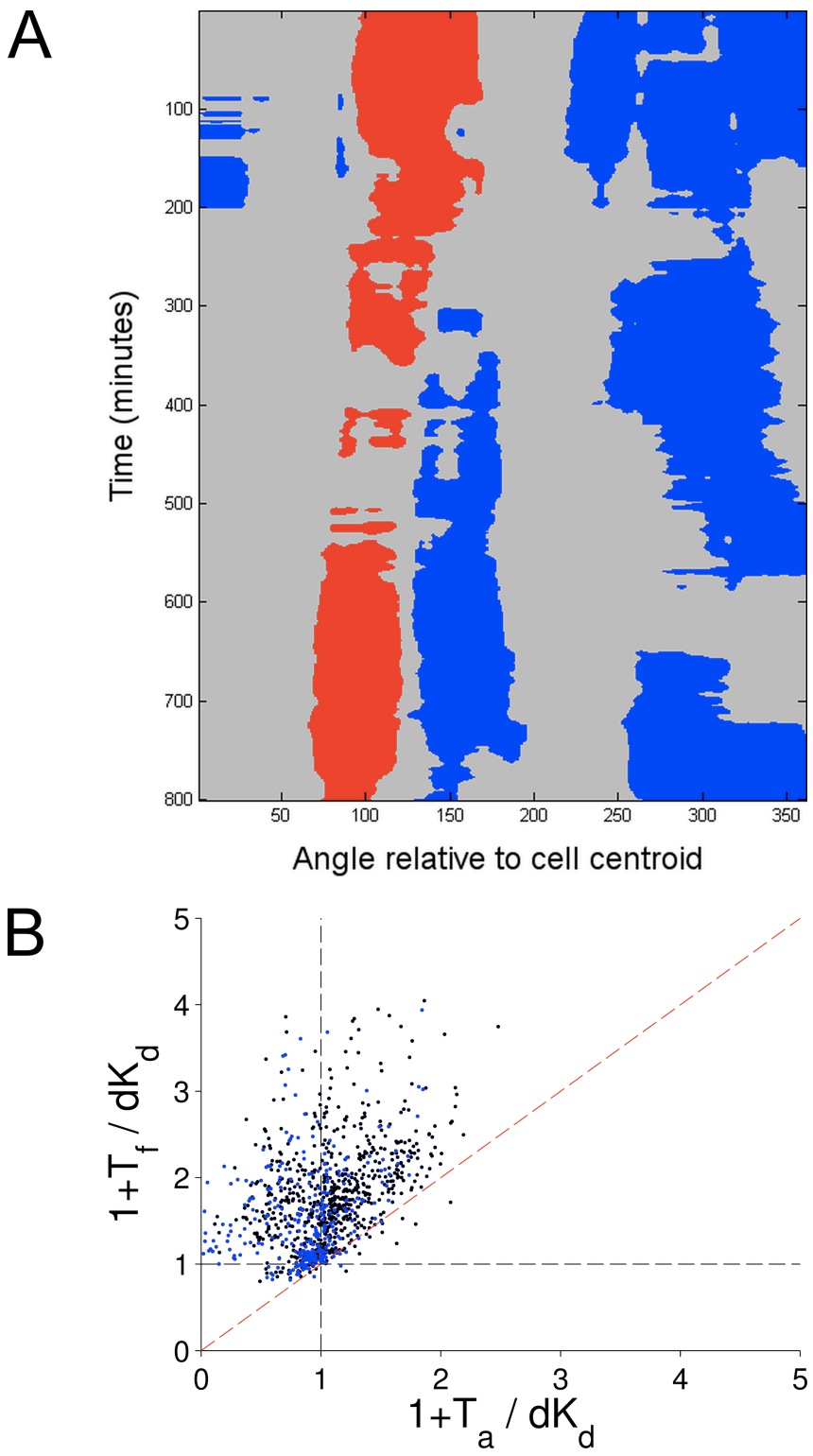

Figure S2. Classification of filopodia according to the motility status of the adjoining membrane region. *a*) Illustration of a representative protrusion/retraction map that was smoothed and subjected to k-means clustering. Red: protruding; gray: stationary; blue: retracting. *b*) Redrawing of Fig. 3D with the filopodia associated with retracting ('rear') regions marked with blue symbols and the others marked with black symbols.